ORIGINAL PAPER

CrossMark

Synthesis of PANI/rGO composite as a cathode material for rechargeable lithium-polymer cells

Rui-Tao Zhang[1] · Jia-Jun Han[1] · Pan Liu[1] · Chang-Yuan Bao[1] · Jin-Ning Cheng[1]

Abstract

Graphene oxide (GO) was synthesized by an improved Hummers method and then reduced with $NaBH_4$; GO became rGO with regular layered structure. Polyaniline (PANI)/rGO composite was prepared by a adsorption double oxidant method with rGO as a template. Some physical characterization methods (Fourier transform infrared spectroscopy analysis, X-ray diffraction, scanning electron microscope, and transmission electron microscope) were used to analyze the morphology and crystallinity of the composite. The electrochemical properties were characterized by cyclic voltammetry, impedance spectroscopy, galvanostatic charge/discharge, and rate capability. The first discharge specific capacity of the rPANI/rGO and PANI/rGO was 181.2 and 147.8 mAh/g. After 100 cycles, the capacity retention rate was still 90.2 and 88.9% separately, and the coulombic efficiency of batteries is close to 100%. These results demonstrate the composite has exciting potentials for the cathode material of lithium-ion battery.

Keywords Polyaniline · Graphene oxide · Composite · Cathode · Lithium battery

Introduction

In 1977, Shirakawa [1] found that the conductivity of polyacetylene could reach a metal level at room temperature when doped with iodine. The discovery aroused great concern for polymers. Since then, people have developed polythiophene [2], polypyrrole [3], polyaniline [4, 5], and other conductive polymer materials. Polyaniline (PANI) has a series of excellent performance, such as corrosion resistance [6], high conductivity [7], good electrochromic performance [8], and a good charge storage performance by mixing the proton acid or salt with reversible self-redox reaction. So it can be used in many fields, such as anti-corrosion materials [9], supercapacitors [10, 11], and secondary batteries [12–14].

As for the current lithium-ion battery cathode materials [15, 16], such as $LiCoO_2$ [17, 18], $LiFePO_4$ [19, 20], $LiMn_2O_4$ [21], and $LiNiO_2$ [22], all have their own shortcomings. And this will limit its widespread application. The properties of high electrochemical activity, good chemical stability, and easy synthesis [23, 24] as well as its unmatched economic

benefit make PANI more suitable for secondary battery electrode materials [25, 26]. But the pure polyaniline newly synthesized is easily agglomerated, affecting the utilization of the material and thereby affecting its physical and chemical properties. Therefore, PANI should be modified by other materials to improve its performance.

Graphene oxide (GO) has a large specific surface area, good electrical conductivity, high intrinsic mobility, and excellent chemical stability [27–29]. Therefore, it is often used to improve the performance of PANI [30, 31]. In this work, the PANI was modified by reduced graphite oxide (rGO), via an adsorption double oxidant method. PANI was coated on the surface of graphene to form a layered structure. Due to the modification of rGO, the physical and chemical properties of PANI were greatly improved.

Experiment

Materials

Graphite powder, potassium persulfate ($K_2S_2O_8$), phosphorus pentoxide (P_2O_5), sulfuric acid (H_2SO_4, 98%), potassium permanganate ($KMnO_4$), hydrogen peroxide (H_2O_2, 30%), sodium carbonate (Na_2CO_3), aniline (AN), manganese sulfate ($MnSO_4$), ammonium persulfate (APS, $(NH_4)_2S_2O_8$), hydrochloric acid (HCl,

✉ Jia-Jun Han
hanjiajunhitweihai@163.com

1 School of Marine Science and Technology, Harbin Institute of Technology, Weihai 264209, China

37%), ammonia ($NH_3 \cdot H_2O$, 28%), manganese sulfate ($MnSO_4$), sodium borohydride ($NaBH_4$, 98%), hydrazine hydrate ($N_2H_4 \cdot H_2O$, 80%), anhydrous alcohol (C_2H_6O) were all analytical grade chemicals and purchased from National Pharmaceutical Group Chemical Reagent Company (No. 52 Ningbo Road, Shanghai, China). Lithium metal foil, aluminum foil, acetylene black, ethylene carbonate (EC), dimethyl carbonate (DMC), styrene-butadiene rubber (SBR, 50%), and lithium hexafluorophosphate ($LiPF_6$) were all battery grade, purchased from Aladdin (Y891 (Branch), Fengxian District, Shanghai, China).

Synthesis of reduced graphite oxide

Graphite oxide was synthesized by an improved Hummers method [32]. In the beaker, 5 g of graphite powder, 2.5 g of $K_2S_2O_8$, 2.5 g of P_2O_5, and 15 mL of H_2SO_4 were mixed evenly and then reacted for 6 h in an 80 °C water bath. One hundred twenty milliliters of H_2SO_4 was added to the product and was stirred together in an ice bath for 30 min. Next, 15 g $KMnO_4$ was slowly added, keep the temperature below 20 °C, and stirred at high speed for 2 h. Once mixed, the temperature of the water bath was raised to 35 °C and reacted for 2 h. Two hundred thirty milliliters of deionized water was added to the solution and stirred for 1 h under 95 °C. Afterwards, 700 mL of distilled water and 25 mL of H_2O_2 were added to the solution. When the color of the solution becomes yellow, the reaction stopped. After filtering and washing for three times, the composite was prepared into 10 mg/mL dispersions (GO dispersions).

In 200 mL of GO dispersions, Na_2CO_3 was added to adjust the pH of the dispersion to 8–9. And then, 15 g of $NaBH_4$ was added slowly at 70 °C in a water bath for 5 to 10 min, followed by stirring at 70 °C for 2 h. The product was dried at 60 °C in a vacuum for 24 h; the rGO was obtained.

Synthesis of PANI/rGO

1.4 g rGO, 200 mL deionized water, 150 mL HCl, and 0.5 g triton were stirred together in an ice bath for 1 h. Seventy grams of aniline monomer and active MnO_2 (50 mL solution containing 10.14 g of $MnSO_4$ and 200 mL solution containing 6.32 g of $KMnO_4$ were stirred at 40 °C for 2 h.) was added in the solution, controlling the reaction temperature below 6 °C for 30 minutes. Afterwards, 1 g APS was added to the solution per minute, repeating 100 times. Meanwhile, deionized ice was added to control the temperature below 5 °C. Once finished, 3 g of acetylene black was added and reacted for 3 h. After washing with deionized water and anhydrous alcohol, the PANI/rGO doped with HCl was obtained.

Deionized water and $NH_3 \cdot H_2O$ mixed solution (volume ratio 3:1) were added into the above preparation of the composite, de-doping reaction at 40 °C for 8 h. After washing with deionized water and anhydrous alcohol and drying for 8 h under vacuum condition, the PANI/rGO composite was obtained.

$N_2H_4 \cdot H_2O$ and PANI/rGO composite at mass ratio of 1:1 were added into an appropriate amount of deionized water and reacted for 12 h in 45 °C water bath. Then, after washing and drying, the rPANI/rGO composite was obtained.

Structure and morphology characterization

Fourier transform infrared (FT-IR) spectra were obtained by a Nicolet 380 FT-IR spectrometer (Thermo Electron Corporation, USA), scanning from 500 to 4000 cm^{-1}. X-ray diffraction (XRD) was recorded by a DX 2700 diffractometer (Dandong Haoyuan Instrument Co., Ltd., China), using Cu K_α radiation ($\lambda = 1.5425$ Å) and scanning from 10° to 80°. Surface morphology and microstructure of powders were analyzed by a field emission scanning electron microscope (FE-SEM MERLIN Compact, Zeiss, Germany) and transmission electron microscope (TEM JEM-2100, JEOL, Japan).
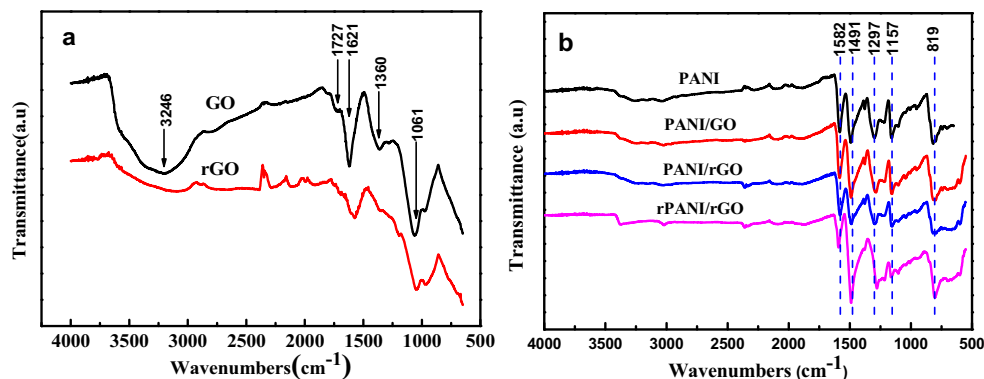
Electrochemical measurements

All the electrochemical performance of the composites was conducted in CR2025-type coin-cell configuration. The composite of the cathode was prepared by coating the mixed slurry of active material (90 wt%) and styrene-butadiene rubber (10 wt%) on aluminum foil, which serves as a current collector. Before assembling the battery, the composite electrode was dried at 80 °C for 12 h under a vacuum. The test cells were assembled in Ar-filled glove box. One molar of $LiPF_6$ dissolved in a mixture of EC/DMC (volume ratio 1:1) was used as lithium-ion electrolyte solution. The specific discharge capacity, coulombic efficiency, cycling performance, and rate capability of the battery were tested by a LAND-CT2001A cycle life tester (Wuhan Jinnuo Instrument Co. Ltd., Wuhan, China) at the cut-off voltages of 2.4–3.8 V. Cyclic voltammetry (CV) was recorded from 2.0 to 4.5 V at the scan rate of 0.5 mV/s. Electrochemical impedance spectroscopy (EIS) was carried out at open circuit potential in the frequency range from 0.01 Hz to 100 kHz. CV and EIS were measured by CHI660E Electrochemical Workstation (CHI660E, Shanghai Chenhua Device Company, China). All electrochemical measurements were carried out at room temperature.

Results and discussion

FT-IR spectroscopic analysis

Figure 1a represents the FT-IR spectra of GO and rGO. The broad and intense peak of GO at 3246 cm^{-1} corresponds to the stretching vibration peak of O-H, indicating that the GO contain large quantity of adsorbed water molecules. Peaks at 1727, 1621, 1061, and 1360 cm^{-1} are the characteristic of the stretching vibration for carbonyl, corresponding to C=O stretching vibrations of

the –COOH group, O-H deformation of the C-OH group, C-OH stretching mode, and C-O-C stretching peak, respectively. However, these peak oxygen functional groups were obviously weakened suggesting that the oxidation degree of GO was heavily decreased. The FT-IR spectra of PANI, PANI/GO, PANI/rGO, and rPANI/GO composite were shown in Fig. 1b. The peaks at 1582 and 1491 cm^{-1} represent the C=C stretching vibration of quinoid and benzenoid structure; its peak intensity ratio represents the degree of oxidation of the PANI. The peaks appeared at 1297 and 1157 cm^{-1} corresponding to the stretching vibration of C-N and C=N, which were a characteristic signature of PANI. The peak at 819 cm^{-1} was assigned to C-C stretching vibration. Since graphene and polyaniline are combined together, the absorption peak coincides with the polyaniline. Compared with the curve of PANI/rGO, the intensity of benzoid ring peaks (1491 cm^{-1}) is greatly increased in the curve of rPANI/rGO, and the quinoid (1582 cm^{-1}) is decreased. This denotes that, after the reduction of hydrazine hydrate, the quinone structure is reduced to a large extent, and PANI was well reduced.

XRD analysis

The crystal structure of PANI/rGO and rPANI/rGO composites was characterized by XRD and shown in Fig. 2. The PANI/rGO pattern reveals three broad crystalline peaks located at $2\theta = 15.2°$, 20.6°, and 24.4°, corresponding to (011), (020), and (200) crystal planes of PANI/rGO, respectively, which is a characteristic diffraction peak of PANI. It indicates that PANI/rGO had been successfully synthesized. Comparing with the PANI/rGO, the rPANI/rGO only have a sharp peak at $2\theta = 19.9°$, which corresponds to the (020) crystal plane of rPANI/rGO. This can be attributed to the crystallinity and the regularity of the PANI/rGO was increased after the reduction of hydrazine hydrate.

Microstructure characterizations

The morphology and structure of GO and PANI/GO composites were investigated by SEM and TEM observations (Fig. 3). The images of GO and rGO were shown in Fig. 3a, b. The

graphene layer of GO is thicker than rGO. And a large block mass appeared in the image of GO, because of the aggregation phenomenon. However, the rGO shows clearly the graphene sheet structure and huge surface area, which is beneficial to the adsorption of PANI. The purified PANI was shown in Fig. 3c; their shapes are twisted which are interlaced with one another because of the aggregation phenomenon. Figure 3d, e shows the morphology of PANI/rGO and rPANI/rGO composites; the PANI/rGO composite is a simple mechanical mixture of PANI and rGO, where the rGO is intercalated between PANI and the chemical bond does not exist. This will make the PANI easily detached from the graphene sheet. As for the rPANI/rGO composite, the rPANI is completely coated on the surface of the rGO to form a layered structure in which the sheets are stacked together. The rPANI and the rGO are bonded together by chemical bonds; it also can be seen from the TEM of rPANI/rGO (Fig. 3f). The rPANI/rGO composite has good morphology and relatively stable structure, so their electrochemical properties should be better.

Electrochemical properties of materials

At a constant current density of 0.2 C, the Li/PANI, Li/PANI/rGO, and Li/rPANI/rGO cells discharging for the first time are shown in Fig. 4a; the specific capacity of the composites is far higher than the pure PANI. The specific capacity of rPANI/rGO composite reached as much as 181.2 mAh/g, which is
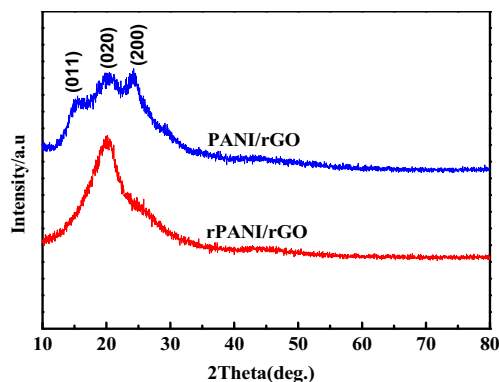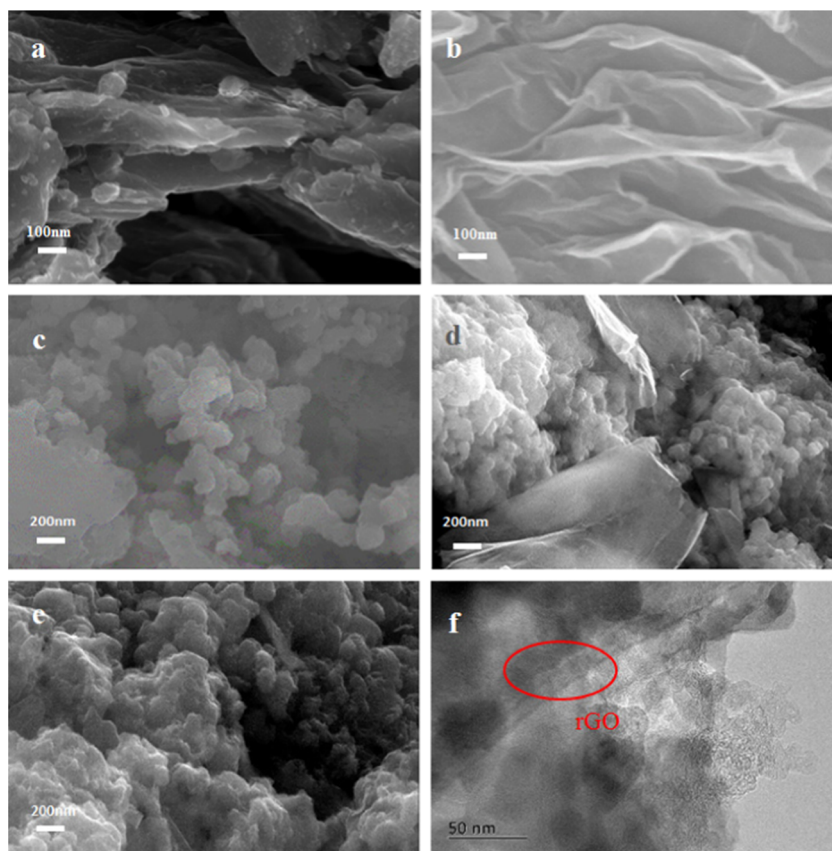

Fig. 2 XRD patterns of PANI/rGO and rPANI/rGO

Fig. 3 SEM images of GO (**a**), rGO (**b**), PANI (**c**), PANI/rGO (**d**), and rPANI/rGO (**e**) and TEM images of rPANI/rGO (**f**)


more than that 22.6% of PANI/rGO composite (147.8 mAh/g). Furthermore, the composites showed excellent cyclability at 0.2 C galvanostatic charge-discharge conditions in Fig. 4b–e. The pure PANI has the lowest capacity and poor cycle performance; it is related to the agglomeration of the material. The rPANI/rGO and PANI/rGO displayed good battery characteristics and maintained 90.2 and 88.9% of capacity after 100 cycle numbers, and the coulombic efficiency was over 97%, respectively. During the whole cycle, the discharge capacity of rPANI/rGO is always higher than that of PANI/rGO. The following explanation can be obtained: for the PANI/rGO composite, PANI intercalated between rGO and without chemical bond, it was prone to agglomeration. The material inside cannot participate in the reaction, resulting in lower utilization of materials. But rPANI/rGO is connected by chemical bonds, the distribution is more uniform, and it has excellent electrochemical performance.

To explore the rate capability of the materials, we selected the rPANI/rGO composites with the best capacity and cycle performance to do the test. The results are shown in the Fig. 4f, The battery of rPANI/rGO delivered a good reversible capacities of 187, 175, 137, 119, and 93 mAh/g at 0.1, 0.2, 0.5, 1, and 2 C respectively. It is obvious that the discharge capacity decreases when the current density increases; the reason is the polarization of electrodes and the lower participation of active materials.

Figure 5 shows the CV plots of two samples at a sweep rate of 0.5 mV/s, with the potential range of 2.0–4.5 V. Metal lithium is used for the reference electrode and counter electrode, and composites are the working electrode. The positive currents are for oxidation and the negative currents are for reduction. The curve of PANI/rGO has a pair of redox peaks: the peak in the top represents the reduction state translated into the oxidation PANI, accompanied by Li^+ or PF_6^- doping process, and similarly, the peak in the bottom expresses the oxidized state transferred to the reduced state and Li^+ or PF_6^- de-doped from the PANI [33, 34]. Comparing with the PANI/rGO, the CV of rPANI/rGO has two pairs of redox peaks, corresponding to the transition of leucoemeraldine base (LEB) to emeraldine base (EB) and pernigraniline base (PNB). Moreover, the rPANI/rGO redox peaks are more acute, indicating that more active substances are involved in the reaction.

In order to study the impedance performance of the composites, the electrochemical impedance spectroscopy (EIS) curves were given in Fig. 6. And the equivalent circuit of electrochemical impedance is analyzed; the values of the component parameters are shown in Table 1 where R_S represents the solution resistance, R_{CT} represents the charge transfer impedance, and CPE1 and CPE2 represent the electric double layer capacitance. From the data fitting in Table 1, it can be seen that the solution resistance of the battery both PANI/rGO and rPANI/rGO is less than 10 Ω, which is only related to the

Fig. 4 **a** Typical first discharging specific capacity of PANI, PANI/rGO, and rPANI/rGO. **b–e** Discharging specific capacity with cycle number. **f** Rate capability of rPANI/rGO
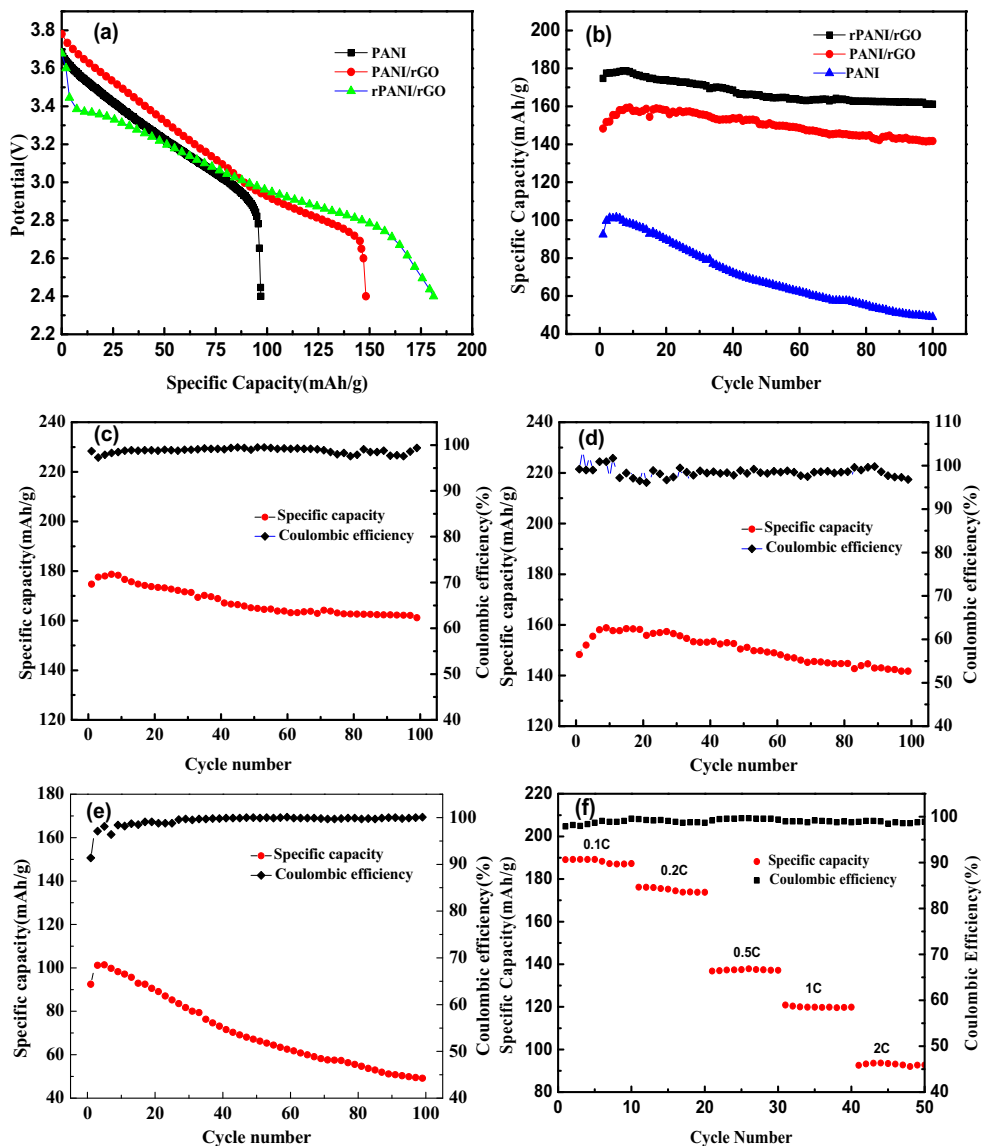
conductivity of the electrolyte. The charge transfer resistance (R_{CT}) is an important electrochemical property of the electrode material. The charge transfer impedance of the PANI/rGO composite is obviously larger than that of the rPANI/rGO, which indicates that the reduced polyaniline material is more conducive to ion doping and de-doping in the event of
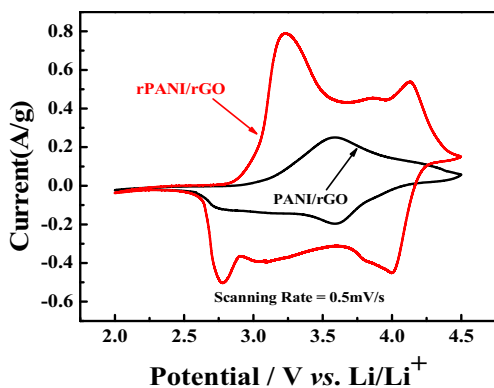

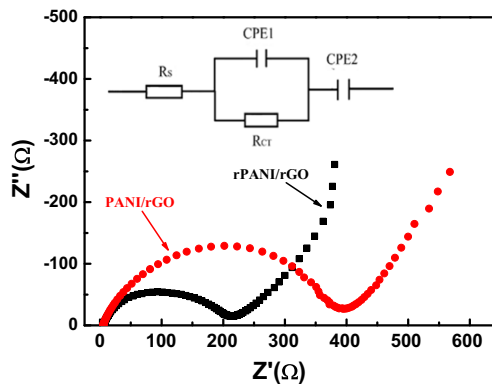Fig. 5 Cyclic voltammetry test of PANI/rGO and rPANI/rGO

Fig. 6 Electrochemical impedance spectra analysis of PANI/rGO and rPANI/rGO

Table 1 EIS curve fitting data of batteries

Composite	R_S (Ω)	CPE1 (10^{-3} F)	R_{CT} (Ω)	CPE2 (10^{-5} F)
PANI/rGO	4.961	16.84	379	2.865
rPANI/rGO	5.368	12.98	188.4	2.292

electrochemical reaction. The reasons may be rPANI/rGO composites have better microstructure and crystallinity, which is beneficial to the doping of ions in the solution.

Conclusion

The PANI/rGO composite was synthesized via an adsorption double oxidant method with rGO as a template. Through physical and electrochemical characterization, we found that the composites have a series of excellent properties. The rPANI/rGO composite formed a layered structure with good morphology and crystallinity. And it reached the high specific capacity up to 181.2 mAh/g, and the capacity retention rate is 90.2%; the coulombic efficiency of batteries is close to 100%. Under the higher discharge rate conditions (1 and 2 C), the rPANI/rGO composite still released a good reversible capacities of 119 and 93 mAh/g. These results demonstrate the composite has exciting potentials for the cathode material of the lithium-ion battery. The reason is that the regular layer structure is of great benefit to active materials participating in the electrochemical reactions. These results illustrate that this kind of composite will have broad prospects as a cathode material for lithium-polymer cells in the future.

References

1. Shirakawa H, Louis EJ, Macdiarmid AG et al (1977) Synthesis of electrically conducting organic polymers: halogen derivatives of polyacetylene, (CH)x. Journal of the chemical society. Chem Commun 16(16):578–580
2. Wochnowski C, Metev S (2002) UV-laser-assisted synthesis of iodine-doped electrical conductive polythiophene. Appl Surf Sci 186(1–4):34–39
3. Qian R, Qiu J (1987) Electrochemically prepared polypyrroles from aqueous solutions. Polym J 18(1–3):13–18
4. Macdiarmid AG, Shao-Lin M, Somasiri NLD et al (1985) Electrochemical characteristics of "polyaniline" cathodes and anodes in aqueous electrolytes. Mol Cryst Liq Cryst 121(1–4):187–190
5. Macdiarmid AG, Chiang J-C, Halpern M, Huang W-S, Mu S-L, Nanaxakkara LD, Wu SW, Yaniger SI (1985) "Polyaniline": interconversion of metallic and insulating forms. Mol Cryst Liq Cryst 121(1–4):173–180
6. Armelin E, Pla R, Liesa F, Ramis X, Iribarren JI, Alemán C (2008) Corrosion protection with polyaniline and polypyrrole as anticorrosive additives for epoxy paint. Corros Sci 50(3):721–728
7. Epstein AJ, Ginder JM, Zuo F, Bigelow RW, Woo HS, Tanner DB, Richter AF, Huang WS, MacDiarmid AG (1987) Insulator-to-metal transition in polyaniline. Synth Met 18(1):303–309
8. Watanabe A, Mori K, Iwasaki Y, Nakamura Y, Niizuma S (1987) Electrochromism of polyaniline film prepared by electrochemical polymerization. Macromolecules 20(8):1793–1796
9. Kalaivasan N, Shafi SS (2017) Enhancement of corrosion protection effect in mechanochemically synthesized polyaniline/MMT clay nanocomposites. Arab J Chem 10(2):S127–S133
10. Wang R, Han M, Zhao Q, Ren Z, Guo X, Xu C, Hu N, Lu L (2017) Hydrothermal synthesis of nanostructured graphene/polyaniline composites as high-capacitance electrode materials for supercapacitors. Sci Rep 7:44562
11. Singu BS, Male U, Srinivasan P et al (2017) Preparation and performance of polyaniline–multiwall carbon nanotubes–titanium dioxide ternary composite electrode material for supercapacitors. J Ind Eng Chem 49
12. Ryu KS, Kim KM, Kang SG, Joo J, Chang SH (2000) Comparison of lithium/polyaniline secondary batteries with different dopants of HCl and lithium ionic salts. J Power Sources 88(2):197–201
13. He BL, Dong B, Wang W, Li HL (2009) Performance of polyaniline/multi-walled carbon nanotubes composites as cathode for rechargeable lithium batteries. Mater Chem Phys 114(1):371–375
14. Liu P, Han JJ, Jiang LF, Li ZY, Cheng JN (2017) Polyaniline/multi-walled carbon nanotubes composite with core-shell structures as a cathode material for rechargeable lithium-polymer cells. Appl Surf Sci 400:446–452
15. Ritchie A, Howard W (2006) Recent developments and likely advances in lithium-ion batteries. J Power Sources 162(2):809–812
16. Fergus JW (2010) Recent developments in cathode materials for lithium ion batteries. J Power Sources 195(4):939–954
17. Ozawa K (1994) Lithium-ion rechargeable batteries with LiCoO2, and carbon electrodes: the LiCoO2/C system. Solid State Ionics 69(3–4):212–221
18. Graetz J, Hightower A, Ahn CC et al (2017) Electronic structure of chemically-delithiated LiCoO2 studied by electron energy-loss spectrometry. J Phys Chem B 106(6):1286–1289
19. Padhi AK, Goodenough JB, Nanjundaswamy KS (1997) Phospho-olivines as positive-electrode materials for rechargeable lithium batteries. J Electrochem Soc 144(4):1188–1194
20. Yi TF, Li XY, Liu H, Shu J, Zhu YR, Zhu RS (2012) Recent developments in the doping and surface modification of LiFePO4, as cathode material for power lithium ion battery. Ionics 18(6):529–539
21. Lee HW, Muralidharan P, Kim DK (2016) Synthesis of one-dimensional spinel LiMn2O4 nanostructures as a positive electrode in lithium ion battery. J Korean Ceram Soc 48(379):379–383
22. Cui P, Jia Z, Li L, He T (2011) Preparation and characteristics of Sb-doped LiNiO2, cathode materials for Li-ion batteries. J Phys Chem Solids 72(7):899–903
23. Gospodinova N, Terlemezyan L (1998) Conducting polymers prepared by oxidative polymerization: polyaniline. Prog Polym Sci 23(8):1443–1484
24. Ameen S, Shaheer Akhtar M, Husain M (2010) A review on synthesis processing, chemical and conduction properties of polyaniline and its nanocomposites. Sci Adv Mater 2(2):441–462
25. Liu Y, Zhou Y, Zhang S, Zhang J, Ren P, Qian C (2016) Amorphous iron phosphate/carbonized polyaniline nanorods composite as cathode material in sodium-ion batteries. J Solid State Electrochem 20(2):479–487
26. Zhou X, He T, Chen X et al (2017) Synthesis and lithium storage properties of vanadium oxide nanotubes (VOxNTs)-polyaniline nanocomposite as cathode material for lithium ion batteries. J Mater Sci Mater Electron:1–10
27. Dreyer DR, Park S, Bielawski CW et al (2014) The chemistry of graphene oxide. Chem Soc Rev 43(15):5288–5301

28. Zhu Y, Murali S, Cai W, Li X, Suk JW, Potts JR, Ruoff RS (2010) Graphene and graphene oxide: synthesis, properties, and applications. Adv Mater 22(45):3906–3924

29. Compton OC, Nguyen ST (2010) Graphene oxide, highly reduced graphene oxide, and graphene: versatile building blocks for carbon-based materials. Small 6(6):711–723

30. Wang H, Hao Q, Yang X, Lu L, Wang X (2010) Effect of graphene oxide on the properties of its composite with polyaniline. ACS Appl Mater Interfaces 2(3):821–828

31. Gui D, Liu C, Chen F, Liu J (2014) Preparation of polyaniline/ graphene oxide nanocomposite for the application of supercapacitor. Appl Surf Sci 307(8):172–177

32. Hummers WS, Offeman RE (1958) Preparation of graphitic oxide. J Am Chem Soc 80(6):1339

33. Sun RK, Man KK, Seong-Gu K et al (2000) The charge/discharge mechanism of polyaniline films doped with LiBF4 as a polymer electrode in a Li secondary battery. Solid State Ionics 135:229–234

34. Ryu KS, Kim KM, Kang SG, Lee GJ, Joo J, Chang SH (2000) Electrochemical and physical characterization of lithium ionic salt doped polyaniline as a polymer electrode of lithium secondary battery. Synth Met 110(3):213–217